Flexible, Conformal Phased Arrays with Dynamic Array Shape Self-Calibration

Austin C. Fikes [1], Amirreza Safaripour, Florian Bohn, Behrooz Abiri, and Ali Hajimiri
Caltech Holistic Integrated Circuits Lab, Caltech, Pasadena, CA 91011, USA
[1]afikes@caltech.edu

***Abstract*— Flexible and conformal phased arrays enable a broad range of novel applications. One of the major challenges for such systems is that they experience a change in their behavior when bent or deformed. A self-calibrating flexible phased array can overcome this by estimating the relative position change of its elements as they undergo local deformations. In this work, we demonstrate a dynamically flexible and conformal 8-element phased array based on a custom CMOS transceiver unit. Beam-steering is demonstrated with the flexible array flat and with the array conformed to convex and concave bend radii of ±120 mm. In addition, we propose and test a shape calibration method that uses only the coupling between elements, using the flexible phase array.**

***Keywords*—flexible electronics, phased array, integrated circuits, integrated circuits, calibration.**

I. Introduction

Flexible, lightweight, and conformal phased arrays open a plethora of new applications ranging from RF active wearables to ultra-light weight space applications and many things in between. Despite their tremendous potential, they present a major challenge, as their electromagnetic performance is intimately tied to the physical dimensions and is thereby affected by shape modifications. For instance, the introduction of a bend in a transmission line can adversely affect a circuit's impedance matching or distort an antenna's radiation pattern. In the past, conformal design has been addressed by designing rigid, conformal RF systems for a specific, pre-determined shape [1]. Obviously, such rigid systems cannot conform to other shapes without a redesign and cannot be used in dynamically flexible systems such as electronics integrated with fabric.

Phased arrays are particularly suited to flexible and conformal applications because they divide a given aperture into smaller elements, each experiencing small local deformation rather than a single large deformation [2]-[3]. These small deformations limit variations in the impedance matching at each element and the element patterns. However, the relative position of the elements must be ascertained to account for the shape deformation in such arrays, instead of calibrating radiator pattern and matching. This self-calibration is critical to proper operation of a flexible phased array system.

A phased array can achieve the desired dynamic flexibility and conformability if it is electromagnetically insensitive to bending and capable of measuring and adjusting for changes in element position as the array deforms. For maximum utility, this shape calibration process should be self-contained, *i.e.*, not reliant on external sensor(s) readout or other sources of information. In [4], an existing flexible phased array, mechanical resistive sensors are used to measure shape deformation. The sensors add an additional interface, significantly increasing the complexity of the overall system. These drawbacks limit the scalability of the array and prevent generic arrays from adopting the calibration scheme.

This work presents a flexible 8-element array with transmit and receive capability and proposes a self-contained shape calibration method using only the coupling between elements in the array. By using the transmit and receive capability to measure the coupling between elements in the array, mechanical deformation of the array is measured.

II. Flexible Phased Array

A. System Overview

The presented 1-D phased array consists of 8 transmitter/receiver custom CMOS integrated circuits operating at 10 GHz, each paired with a radiator. All transceivers are phase locked to a shared reference signal. Fig. 1 shows the flexible phased array. The phased array is built on a flexible 4-layer polyimide and copper circuit board (total thickness ~12 mil). One side of the board holds the custom CMOS IC, reference distribution network, and interface circuitry while radiators are mounted on the other side. The radiator-side ground plane isolates the radiators from the other components. The components were positioned to maintain flexibility around the axis along which the beam may be steered.

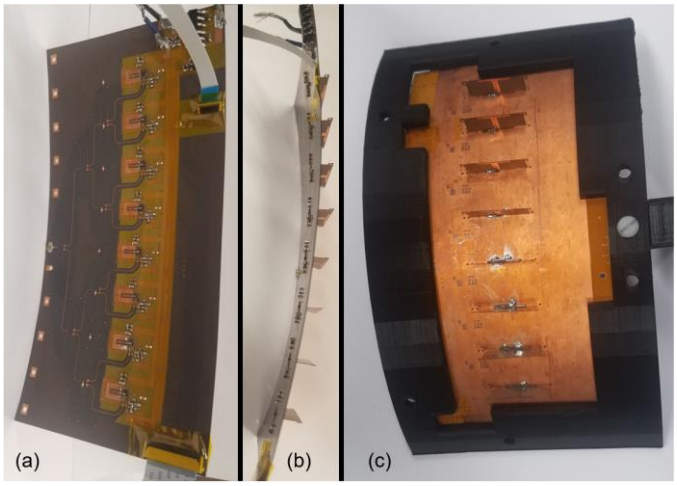

Fig. 1. Flexible Phased Array: (a) Circuit component side of flexible phased array. (b) In-plane view of flexible phased array. (c) Radiator side of flexible phased array.

B. *Bend Tolerant Radiator*

The ideal radiator for a conformal phased array should possess a broad, near-hemispherical radiation pattern oriented normal to the conformed surface and have low sensitivity to bending in impedance matching and pattern. Ground plane backed dipoles satisfy these requirements for a 1-D array. Each radiator is made from a single polyimide and copper sheet soldered to the 4-layer phased array board, as shown in Fig. 2a. The element pitch is 18 mm (0.6λ at 10 GHz) when the array is flat. The antenna feed connects to a single-ended coplanar transmission line leading to the CMOS IC. The feed from the board to the radiating arms acts as a balun to drive the dipole differentially.

The volume above the ground plane and directly below a dipole's radiating arms does not experience significant deformation with bending. Because the strongest electric fields are contained in this region, the radiator is less sensitive to bending. Fig. 2b and Fig. 2c present the measured pattern of the 4th element in the array when the array is flat and when it is convexly conformed to a bend radius of 120 mm. The similarity of the pattern with and without bending illustrates the radiators' low sensitivity to bending.

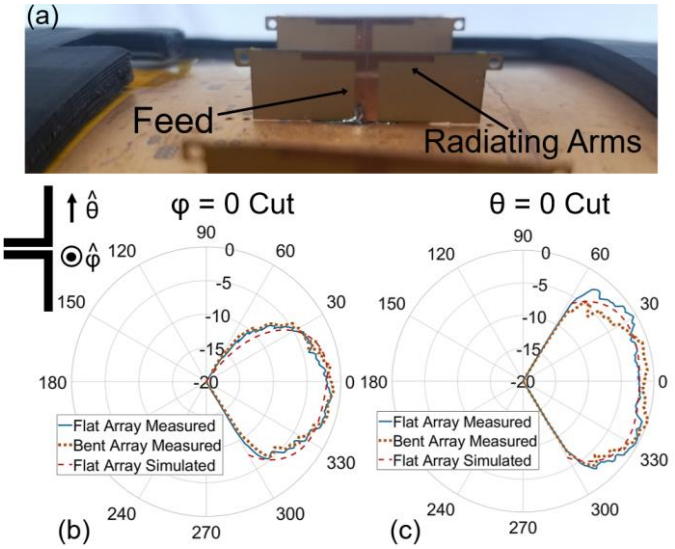

Fig. 2. Radiator Element: (a) Radiators of the array are shown while the array is subjected to a 120mm bend radius deformation. (b) φ = 0 cut patterns from -60° to +60° of the 4th element of the array, measured when the array is flat and when it is bent at a 120mm bend radius. (c) θ = 0 cut patterns. Both pairs of patterns are normalized (dB) to the global maximum which occurs in the Bent Array, θ = 0 Cut. The simulated patterns are normalized to 0 degrees values of the flat measured results. The measured field is linearly polarized in the +θ direction.

C. *Transmitter/Receiver Integrated Circuit*

The custom CMOS RFIC is responsible for generating and transmitting a high-power 10 GHz signal, as well as receiving incident signals and down-converting them to baseband. The high-level block diagram of the IC is shown in Fig. 3a. The IC uses a 2.5 GHz reference signal, which is converted to 10 GHz by an on-chip phase-locked loop (PLL) with a fixed 4x multiplication ratio. The output lock range of the PLL exceeds 9.9 GHz - 10.4 GHz. At 10 GHz the IC can either transmit the signal using an integrated power amplifier (PA) or convert a received signal to baseband through a direct down-conversion receiver. The functions of the IC are controlled through a digital interface.

A large NMOS switch between the outer balun arm and ground allows the receiver to see a higher impedance when the PA is not operating. The receiver is unmatched but has sufficient dynamic range for the high-power inter-element coupling measurements used for shape calibration. By keeping the NMOS switch closed and enabling the PA, the RFIC is capable of taking a self-loop measurement (measuring its own output), which is used in the calibration process. There are two independent phase control systems in the IC, each separately offering greater than 2π phase control. The first is the PLL-based phase control that controls the phase of the transmitted signal and the receiver mixer LO. The second is an IQ phase rotator before the PA, which only affects the transmitted phase. The phase rotator can be programmed from an on-chip SRAM, allowing data to be rapidly modulated onto the transmitted signal. The IC is implemented in TSMC's 65nm CMOS process and the die photo can be found in Fig. 3b.

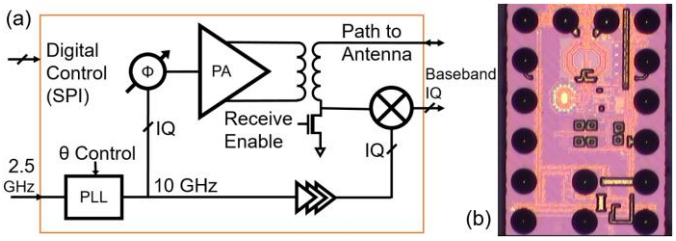

Fig. 3. Transmit/Receive RFIC: (a) Integrated circuit block diagram. (b) Die photo.

III. Coupling Shape Calibration

The proposed coupling shape calibration uses mutual coupling between elements to determine array shape. Mutual coupling has previously been used for phase calibration of rigid arrays [5] but has not been explored as a shape calibration technique. As a flexible phased array is deformed, the relative positions of its radiating elements changes. By measuring the distance between elements, the shape of the array can be reconstructed. Flexible phased arrays naturally adapt frequency modulated continuous wave (FMCW) radar as a distance measuring tool that can be implemented without significant overhead to the array.

Ideally, a bistatic radar measurement, which measures the coupling path between two elements in the array, would be sufficient to determine the distance between elements. However, several non-idealities can hinder this measurement. In an array that is sufficiently dense to avoid grating lobes, the element pitch is on the order of 0.5λ. This short distance limits the amount of phase accumulated at baseband by the radar measurement between elements. Standard linear FMCW radar would observe a small fraction of a full period of the baseband frequency corresponding to this return. Compounding the difficulty of measuring these short distances is the frequency-dependent phase response of active and passive components (such as amplifiers and transmission lines). The phase change

of these components from the beginning to the end of an RF chirp is insignificant in typical FMCW applications where the baseband signal extends for many cycles, dwarfing their effect. However, in short distance measurements, the phase change of these components over the chirp bandwidth is comparable to the phase change of the radiation path.

Unlike standard FMCW measurements, the proposed calibration procedure measures total phase accumulated in the radiation path between the beginning and end frequencies of interest. This phase accumulation will be less than 2π for small element separation, which is why phase is measured rather than frequency. When this phase accumulation is less than a cycle, phase wrapping is not a concern, allowing unambiguous static single frequency measurements at multiple frequency points, for instance, at the beginning and end points of the chirp bandwidth. This removes the need for a chirp-able phase reference signal and avoids challenges associated with chirp non-linearity and PLL loop dynamics present in standard FMCW. For arrays large enough to experience phase wrapping while measuring between elements, additional frequency points along the bandwidth may be used. To account for components before and after the radiation path, the calibration procedure requires self-loop measurements in which a single element acts as transmitter and receiver. This self-loop measurement can be subtracted from the coupling measurement to calibrate out the effect of these components from the measurement.

A simplified model of the self-calibration set-up is shown in Fig. 4. Transfer function, $H_{tx}(f)$, represents components only in the transmit path, such as the phase rotator and PA, while $H_{rx}(f)$ represents components only in the receive path, such as the LO buffer chain. The beginning and the end of the measurement bandwidth is f_1 and f_2, respectively. The goal of the calibration procedure is to measure the phase difference, $\angle H_{AB}(f_2) - \angle H_{AB}(f_1)$, which is the phase accumulated over the chirp bandwidth and is related to the distance between elements A and B. The procedure assumes $\angle H_{AB}(f)$ is symmetric, as traveled from A to B or B to A, knowing only passive elements lie in that path (reciprocity).

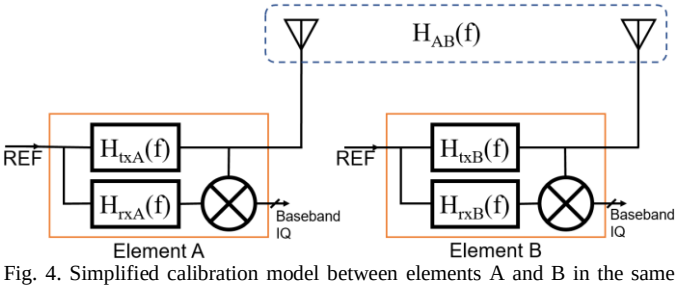

Fig. 4. Simplified calibration model between elements A and B in the same flexible phased array.

The calibration procedure first measures the phase of the coupling between the elements with A as the transmitter and B as the receiver, $\angle\theta_{AB}(f)$, namely,

$$\angle\theta_{AB}(f) = \angle H_{txA}(f) + \angle H_{AB}(f) - \angle H_{rxB}(f). \quad (1)$$

Next, the calibration procedure measures the element A self-loop to find $\angle\theta_{AA}(f)$ as follows:

$$\angle\theta_{AA}(f) = \angle H_{txA}(f) - \angle H_{rxA}(f). \quad (2)$$

After $\angle\theta_{BA}(f)$ and $\angle\theta_{BB}(f)$ are measured, the procedure calculates $\angle H_{AB}(f)$ by

$$\angle H_{AB}(f) = (\angle\theta_{AB}(f) + \angle\theta_{BA}(f) - \angle\theta_{AA}(f) - \angle\theta_{BB}(f))/2 \quad (3)$$

After this set of measurements have been performed at f_1 and f_2, $\angle H_{AB}(f_2) - \angle H_{AB}(f_1)$ is calculated.

To measure the shape of the flexible phased array, this procedure can be performed between all elements in the array. If the distance between all elements is measured, the resultant system of equations is likely over-defined. This additional information can be used to reduce uncertainty. Furthermore, some array deformations may break line-of-sight between two elements that are far apart in the array. For large-scale arrays measuring all element pairs may be prohibitively time consuming. In these cases a subset of element pair measurements can be performed and used. This subset should be chosen to span the space of possible curvatures.

This calibration scheme assumes no significant objects in the near-field of the array. It should be noted this calibration method does not account for changes in the phase response of the components before and after the transmit and receive path split within each element such as the reference distribution network, antenna, and feed line. These components can be simulated or measured separately. Furthermore, the effect on the measurement of manufacturing variation in these components is mitigated by the measurements' differential nature: the calibration procedure measures the difference in phase at the beginning and end of the measurement bandwidth rather than absolute phase at any point. While demonstrated in a 1-D array, this calibration method can be naturally extended to 2-D and 3-D array calibration.

IV. Measurements

A. Array Performance

The beam-steering capability of the flexible phased array is demonstrated in Fig. 5. The figure shows the normalized gain pattern measurement for a steered beam when the array is flat and when it is conformed to a convex 120 mm bend radius.

The element phases for beam-steering were determined through a coarse optimization procedure. The patterns are taken at the center of the bandwidth used for shape calibration measurements, *i.e.* 10.176 GHz.

B. Shape Calibration Measurement

Shape calibration measurements were performed for the array when flat and when conformed to convex and concave bends. When bent, the phase centers of the radiators are moved farther apart or closer together. This change in distance is measurable through shape calibration. The measurement is taken between 9.936 GHz and 10.416 GHz for a bandwidth of

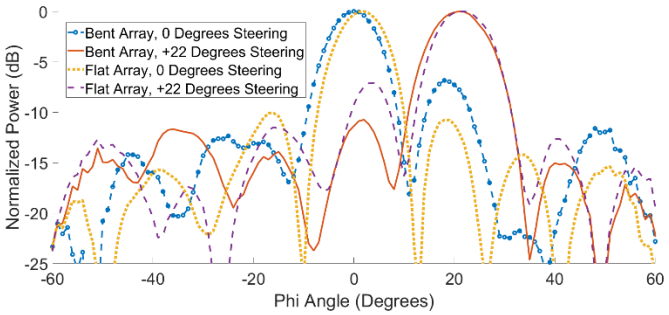

Fig. 5. Beam-steering pattern measurements from -60° to +60° for flat and convexly conformed array. Each pattern is normalized to its highest measured value.

480 MHz. Each measurement is repeated for 24 phase rotator settings allowing for receiver nonlinearity correction [6]. Adjacent element coupling was measured with the on-chip balun switch closed, but non-adjacent element coupling was measured with the switch open to provide sufficient signal at the receiver. This introduces a systematic difference between the self-loop measurements and coupling measurements for non-adjacent elements. This is corrected by measuring the difference between the switch-open and switch-closed received phase for each element while receiving from an adjacent element, then subtracting this difference from the results. Fig. 6 presents the calibration measurement results for the array when flat and when bent convexly and concavely to 120 mm bend radius. Because the deformation applied to the array is symmetric, it is assumed the distance between each element changes by a similar amount. With this assumption, the results for each possible element spacing (one element apart, two elements apart, *etc.*) are averaged together and presented as a single data point. The y-axis of Fig. 6 shows the phase accumulated between 9.936 GHz and 10.416 GHz in the radiation path for the element spacing listed on the x-axis.

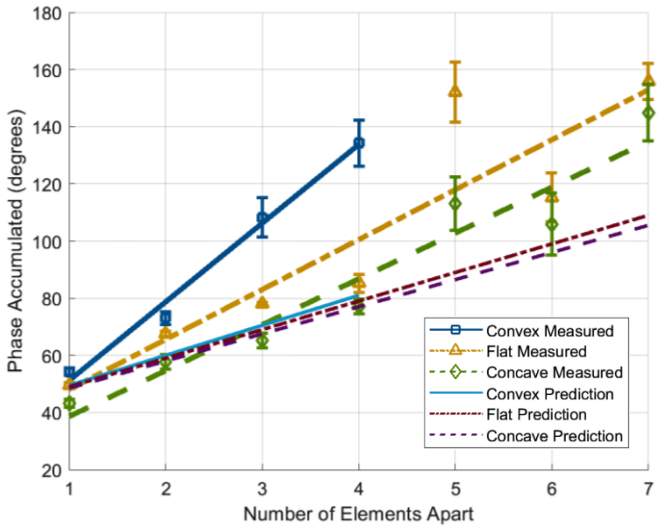

Fig. 6. Shape calibration measurements for bent and unbent array (120 mm bend radius). Linear regression best fit lines are plotted for each of the measured array shapes. Each measured data point represents the average of six separate measurements. The error bars show the standard deviation of the measurement for a given element separation. The convex measurements at element separations above 4 are not included because the bend has moved the elements out of line-of-sight.

In addition to the measured data, three lines representing phase accumulation of a simplified free space model, where phase is linearly related with distance are plotted. The slope of the flat free space model is 10 degrees per element spacing as calculated using the bandwidth of the measurement and the element pitch. The y-intercept of the free space model is determined from an electromagnetic simulation of the coupling between adjacent elements in a flat array. The simulation found 49 degrees as the expected phase accumulation for adjacent elements. The convex and concave bent measurements remain above and below the flat measurements for all element spacings, respectively, correctly indicating the direction of the bend.

This measurement shows the viability of this approach for flexible conformal array shape calibration.

V. Conclusion

This paper presents an 8-element, dynamically flexible and conformal, 1-D, phased array operating at 10 GHz. The array is assembled using a custom CMOS RFIC. The radiator elements are insensitive to bending, and beam-steering capability is demonstrated when the array is flat and when it is bent. A method for flexible phased array shape calibration using the coupling between elements is proposed. The presented array is used to demonstrate the shape calibration method.

Acknowledgment

The authors wish to thank their funders and collaborators at the Caltech Space Solar Power Initiative, as well as M. R. Hashemi, D. Hodge, C. Ives, and A. Ngai who aided in measurement set-up and manuscript preparation.

References

[1] Y. Zhao, Z. Shen, and W. Wu "Conformal SIW H-Plane Horn Antenna on a Conducting Cylinder," *IEEE Antennas and Wireless Propagation Letters*, vol.14, pp. 1271-1274, Feb. 2015.

[2] P. Knott, T. Bertuch, H. Wilden, O. Peters, A. R. Brenner, and I. Walterscheid., "SAR Experiments Using a Conformal Antenna Array Radar Demonstrator," *International Journal of Antennas and Propagation*, vol. 2012, Article ID 142542, 2012.

[3] K.S. Beenamole, Sreejith C. A., G. Shankar, "Studies on conformal antenna arrays placed on cylindrical curved surfaces," in *2016 International Symposium on Antennas and Propagation*, 2016, p. 75.

[4] B. Braaten, S. Roy, S. Nariyal, M. Aziz, N. Chamberlain, I. Irfanullah, M. T. Reich, and D. Anagnostou, "A Self-Adapting Flexible (SELFLEX) Antenna Array for Changing Conformal Surface Applications," *IEEE Transactions on Antennas and Propagation*, vol. 61, pp. 655-665, Feb 2013.

[5] H. M. Aumann, A. J. Fenn, and F. G. Willwerth, "Phased Array Antenna Calibration and Pattern Prediction Using Mutual Coupling Measurements," *IEEE Transactions on Antennas and Propagation*, vol. 37, pp. 844-850, Jul 1989.

[6] S.W. Ellingson. (2013) Correcting I-Q Imbalance in Direct Conversion Receivers webpage on Virginia Tech ECE. [Online]. Available: https://www.faculty.ece.vt.edu/swe/argus/iqbal.pdf